Cluster Compounds

Deutsche Ausgabe: DOI: 10.1002/ange.201504473
Internationale Ausgabe: DOI: 10.1002/anie.201504473

Finding the Most Catalytically Active Platinum Clusters With Low Atomicity**

*Takane Imaoka, Hirokazu Kitazawa, Wang-Jae Chun, and Kimihisa Yamamoto**

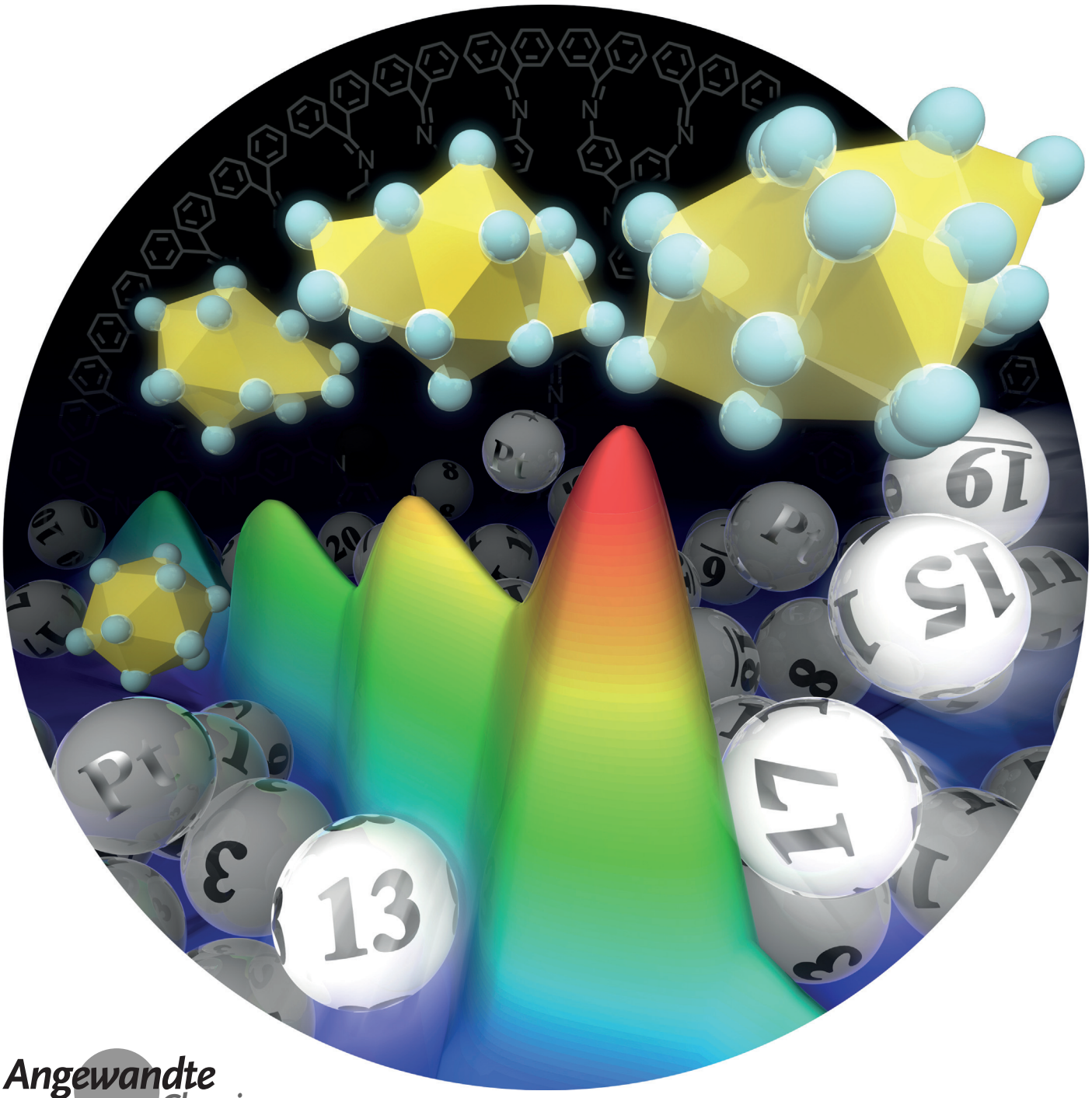

Abstract: *On a subnanometer scale, an only one-atom difference in a metal cluster may cause significant transitions in the catalytic activity due to the electronic and geometric configurations. We now report the atomicity-specific catalytic activity of platinum clusters with significantly small atomicity, especially below 20. The atomic coordination structure is completely different from that of the larger face-centered cubic (fcc) nanocrystals. Here, an electrochemical study on such small clusters, in which the atomicity ranged between 12 and 20, revealed Pt_{19} as the most catalytically active species. In combination with a theoretical study, a common structure that leads to a high catalytic performance is proposed.*

As much smaller analogues of metal nanoparticles, metal clusters on a subnanometer size scale have attracted significant attention over the past decades because they occasionally exhibit significant catalytic activity.[1] One of the important concepts in recent cluster science is the superatom, which behaves as if it were a different element.[2] Although superatoms generally have spherical symmetry, a recent study by Castleman and colleagues indicated the prospect for the prominent reactivity of less symmetric clusters, as exemplified by a study on the unique reactivity of Al_{17}^- in the gas phase.[3] How are the activities of less symmetric clusters as catalysts? To answer this question, precise synthesis at almost a one-atom resolution is necessary. However, there has been no synthetic method available to allow one-atom precision, except for the especially stable magic number clusters.[4]

A dendrimer-based template synthesis has been developed for small nanoparticles (1–2 nm) with a narrow size polydispersity.[5] The significant advantage is that the average particle size is configurable based on the stoichiometry between the dendrimer and the precursor metal salts (or ionic complexes), but not the intrinsic stabilities of the target clusters. We have recently improved the method to form metal clusters with precise atomicity, and revealed the significant difference in the catalytic activity between only one-atom-different clusters (Pt_{12} and Pt_{13}).[6,7] The employment of phenylazomethine dendrimers could provide a breakthrough of the precision limit for the generalized nanoparticle-based approach and allow the production of subnanoparticles with precise atomicity.

In this study, various platinum subnanoparticles (clusters) were synthesized and their catalytic activity for the oxygen reduction reaction (ORR) was compared. The reduction of oxygen molecules is a fundamental chemical process for various industrial applications such as the cathode reaction of a fuel cell[8] or the aerobic oxidation of organic molecules.[9] It has long been considered that a platinum nanoparticle catalyst loses its catalytic activity when the nanoparticle diameter is less than 2 nm. This could be reasonably explained by an upward shift of the d-band center with the size reduction, which would lead to a stronger oxygen–platinum binding energy. Previous experimental results have supported this concept.[10] However, a nonmagic-number subnanometer cluster may have nonperiodic surfaces, that are unavailable on bulk or larger nanoparticles, which suggests that the catalytic activities of the platinum subnanoparticles are not linearly dependent on the atomicity, but on the atomicity-specific properties.

Cluster catalysts with a definite number of platinum atoms were synthesized using a fourth-generation dendritic phenylazomethine with a triphenylpyridylmethane core (**DPAG4-PyTPM;** Figure S1) based on a previously reported procedure.[11] The basic approach to synthesize the subnanoparticles involves two steps. The first step is the formation of platinum chloride ($PtCl_4$) complexes assembled inside the dendrimer, whereas the second step is the chemical reduction of the complexes to afford the corresponding metal nanoparticles with definite atomicity in the dendrimer. An almost monodisperse magic number platinum cluster (Pt_{13}) was synthesized when 13 equivalents of $PtCl_4$ was complexed in **DPAG4-PyTPM** ([$PtCl_4$]/[**DPAG4-PyTPM**] = 13).[7] The significant advantage of the phenylazomethine dendrimers as the template ligand is the precise control of the atomicity to obtain consistent nanoparticles and subnanoparticles at almost one-atom resolution. As previously reported,[11] **DPAG4-PyTPM** undergoes a unique stepwise complexation process (Figure S2) that includes multistep shifts of the isosbestic points at 1, 2, 5, 13, 17, 29, and 37 equivalent additions of the metal chloride. At each point at which the isosbestic point shifts, a deviation in the number of assembled metal complexes is minimized, in principle. In particular, the 13- or 17-$PtCl_4$ assembly in **DPAG4-PyTPM** ([$PtCl_4$]/[**DPAG4-PyTPM**] = 13 or 17) is a specifically focused

[*] Dr. T. Imaoka,[+] Dr. H. Kitazawa,[+] Prof. Dr. K. Yamamoto
Chemical Resources Laboratory, Tokyo Institute of Technology
Yokohama 226-8503 (Japan)
E-mail: yamamoto@res.titech.ac.jp
Prof. Dr. W.-J. Chun
Graduate School of Arts and Sciences
International Christian University
Mitaka, Tokyo 181-8585 (Japan)
[+] These authors contributed equally to this work.

[**] This study was supported by the CREST program of the Japan Science and Technology (JST) Agency. XAFS measurements were conducted at the BL9C and BL12C beamlines of the High Energy Accelerator Research Organization—Institute of Materials Structure Science—Photon Factory (KEK-IMSS-PF) under the approval of the Photon Factory Advisory Committee (Nos. 2011G687 and 2013G568) and BL01B1 of SPring-8 with the approval of the Japan Synchrotron Radiation Research Institute (JASRI) (Proposal numbers 2014B1406 and 2014A1326). We also appreciate technical support (electrochemical in situ XAFS cell) from the Technical Division of Catalysis Research Center (S. Mukai), Hokkaido University. We thank the staff of the Photon Factory and Spring-8 for technical support. A part of this study was supported by the National Institute for Materials Science (NIMS) microstructural characterization platform (NMCP) as a program of the "Nanotechnology Platform" of the Ministry of Education, Culture, Sports, Science and Technology (MEXT) (Japan). We are grateful to Dr. Y. Nemoto for assistance with the high-resolution STEM observations, and D. Suzuki for assistance with the electrochemical measurements.

Supporting information for this article is available on the WWW under http://dx.doi.org/10.1002/anie.201504473.

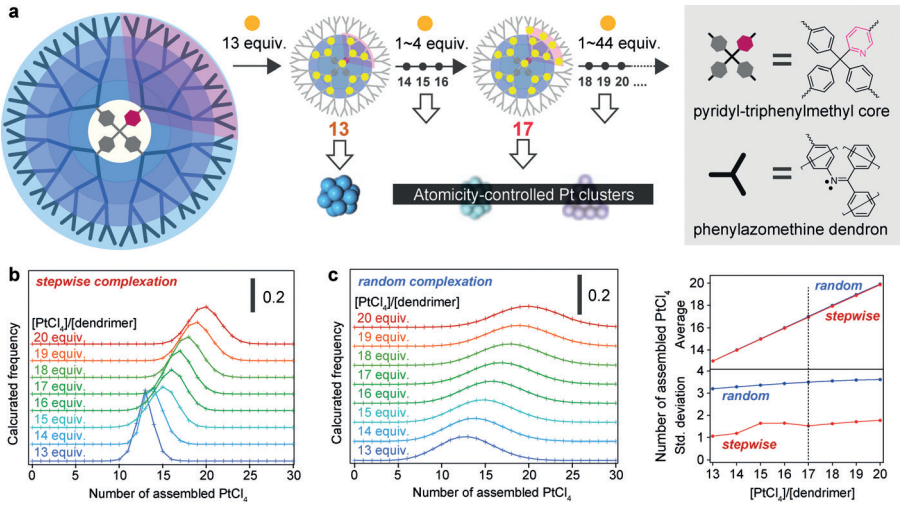

Figure 1. A dendrimer reactor for the precise synthesis of atomicity-consistent Pt clusters. a) The DPAG4-PyTPM dendrimer has 61 coordination sites (1 pyridyl and 60 phenylazomethines) and undergoes an irregular stepwise complexation process with metal chlorides (e.g., $GaCl_3$ or $PtCl_4$). The dendrimer is designed to obtain an almost monodispersed 13 $PtCl_4$-assembling complex upon the addition of 13 equivalents of $PtCl_4$. b) The calculated number distribution of the assembled $PtCl_4$ molecules in each dendrimer is based on equilibria and statistical simulation. This simulation assumes the binding constant to each imine site as follows: K_1, $K_2 = 10^{11}\ M^{-1}$ for the first 5 $PtCl_4$ bindings, $K_3 = 10^{9}\ M^{-1}$ for the 6th to 13th binding, $K_4 = 10^{7}\ M^{-1}$ for the 14th to 17th binding, and $K_5 = 10^{6}\ M^{-1}$ for the 18th to 29th binding. Bindings beyond the 29th are considered to be much weaker and were thus ignored in this simulation. c) A simulation result assuming equivalent bindings ($K = 10^{8}\ M^{-1}$) to every 61 coordination sites in a dendrimer.

number of the metal assembly, at which the number of assembled metals in the dendrimers would have the smallest polydispersity. For example, the binding constants to the respective imine sites are presumed to be within a difference of two orders of magnitude between neighboring layers.[12] The statistical and equilibrium simulation (Figure 1b) suggested that the standard deviation in the number of assembled metal precursors would be the minimum value ($\sigma = 1.05$) at $[PtCl_4]/[dendrimer] = 13$ (Figure 1d). Even if the stoichiometry moves to higher values ($[PtCl_4]/[dendrimer] > 13$), the σ values remain relatively low ($\sigma < 1.8$). These deviations are substantially lower than that expected in a randomly coordinating system ($\sigma > 3.1$), which suggests good resolution in the present atomicity-dependent analysis. In this study, Pt_n ($n =$ 12–24) clusters were synthesized using both **DPAG4-PyTPM** and polyamidoamine (**PAMAM G4-OH** in Figure S1) dendrimer templates with stepwise and random processes, respectively.

Precursor complexes with various $[PtCl_4]/[dendrimer]$ stoichiometry (dendrimer: **DPAG4-PyTPM**) were prepared, and each complex was reduced with $NaBH_4$ to produce the corresponding platinum clusters. A similar template synthesis with **PAMAM G4-OH** using K_2PtCl_4 as the platinum source was performed according to a method in the literature.[13] Low-magnification high-angle annular dark-field scanning transmission electron microscopy (HAADF-STEM) images of the product clusters by both dendrimers (Figures 2a and S3) showed almost monodisperse platinum subnanoparticles prepared using both dendrimers (**DPAG4-PyTPM** and **PAMAM G4-OH**). The mean particle size was 0.8 nm and the standard deviation was only ± 0.2 nm when $[PtCl_4]/[dendrimer]$ was 19. The possible origins of these particle-size deviations are the inevitable artifact on the image processing and the cluster deformation during the STEM observations. This result apparently supports the idea that these subnanoparticles are almost monodisperse.

Stoichiometric production of the clusters was confirmed by electrospray time-of-flight mass spectrometry (ESI-TOF-MS) measurements using the previously reported ligand exchange method.[7] The CO-protected Pt_{13} cluster, which was derived from the as-synthesized Pt_{13} in **DPAG4-PyTPM**, exhibited a single peak attributed to $[Pt_{13}(CO)_{15}]^{2-}$.[7] Similar to a method for the Pt_{13} cluster synthesis, carbon monoxide gas was introduced into the reaction vessel containing the Pt_{19} cluster solution just after reduction of the $[PtCl_4]/[\mathbf{DPAG4\text{-}PyTPM}] = 19$ assembly. A spectrum of the resulting solution (Figure 2c) shows the most intense peak at 2147.15 accompanied by many isotopes with 0.5 Da intervals, which is characteristic of divalent platinum cluster anions. The distribution pattern of the isotopes around the main peak is equivalent to the calculated isotropic distribution of $[Pt_{19}(CO)_{21}]^{2-}$. Besides the main peak, similar divalent peaks accompanying similar isotopes and fragmentations were observed, each of which corresponds to $[Pt_n(CO)_{n+2}]^{2-}$ ($n =$ 16–22). Based on the simplified assumption that the cluster yields correlate to the intensity in the mass spectrum, the visible distribution of the cluster atomicity is in good agreement with the distribution expected from the simulation (Figure 1b,d). It should be noted that a similar ESI-TOF-MS analysis conducted without the dendrimer template (Figure 2c) showed a series of various cluster anions all attributed to $[Pt_n(CO)_{n+2}]^{2-}$ ($n =$ 13–20), which suggests that each larger cluster ($n > 13$) has a stable icosahedral Pt_{13} kernel, to which several excess Pt adatoms are attached. All valence electrons accompanying the metal–metal bonding can be counted based on the Wade–Mingos–Lauher electron counting rule. For example, the number of cluster valence electrons (CVEs) for the observed $[Pt_{13}(CO)_{15}]^{2-}$, $[Pt_{14}(CO)_{16}]^{2-}$, $[Pt_{15}(CO)_{17}]^{2-}$, and $[Pt_{16}(CO)_{18}]^{2-}$ anions are 162, 174, 186, and 198, respectively. The 162 CVE suggests an icosahedral platinum cluster,[14,15] and a +12 CVE increase by the addition of one platinum atom to each anion can be interpreted as the attachment of a new platinum atom at the three-fold hollow sites through the face-sharing condensation with Pt_4 tetrahedra.[16] A recent X-ray absorption fine structure (XAFS) and pair distribution function (PDF) study[17] showed that the surface coordination by CO molecules only induces small

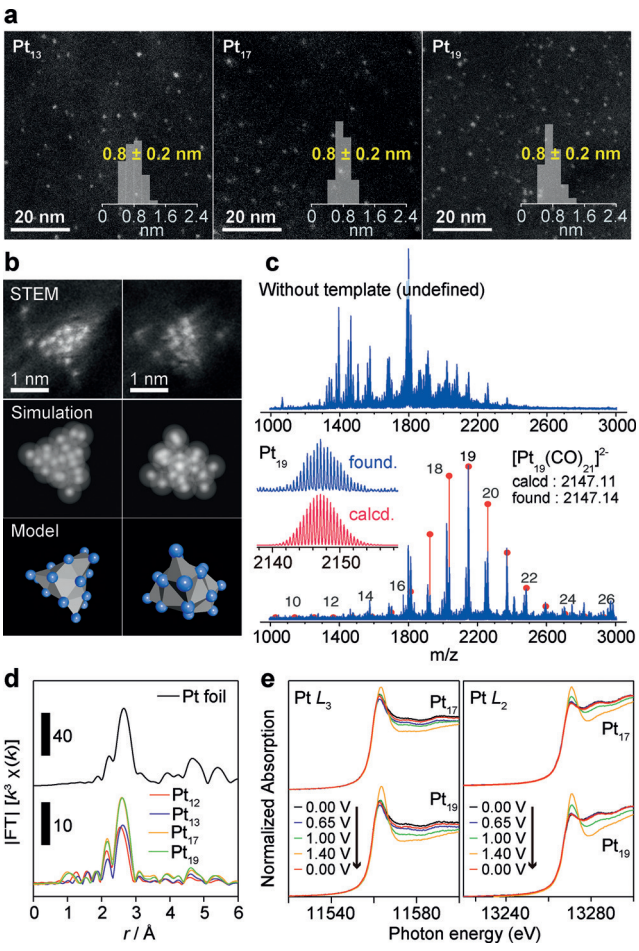

Figure 2. Characterization of platinum clusters synthesized with **DPAG4-PyTPM**. a) Low-magnification HAADF-STEM images (200 kV) of Pt_{13}, Pt_{17}, and Pt_{19} clusters supported on graphene sheets. Insets show histograms of the particle diameters. b) High-magnification aberration-corrected HAADF-STEM snapshots (80 kV) of a Pt_{19} cluster. Simulation: HAADF-STEM z-contrast simulation of the structure model. Model: expected structural model for Pt_{19} optimized by DFT calculations. c) Negative-mode ESI-TOF-MS spectra of Pt_{19} and undefined clusters synthesized without the dendrimer template as the CO-protected forms. Red bars with markers superimposed on each spectrum indicate the expected distribution of atomicity based on the simulation shown in Figure 1b. d) Fourier-transformed k^3-weighted Pt L_3-edge EXAFS spectra for Pt_{12}, Pt_{13}, Pt_{17}, and Pt_{19} supported on graphitic mesoporous carbon. e) Pt L_3- and L_2-edge XANES spectra measured in situ under electrochemical conditions. Constant potentials (0, 0.65, 1.00, 1.40 V vs. Ag/AgCl) were applied in turn to the cluster samples mounted on a working electrode (carbon felt). The potential was then finally set back to 0 V.

extensions of the Pt–Pt bonds without any structural rearrangement, even if the cluster size is as small as 1 nm, although a longer reaction time would lead to different CO-rich clusters.[18] These results support the idea that the cluster structure can be discussed based on the corresponding CO-protected derivatives. We have employed as-synthesized clusters for extended XAFS (EXAFS) analyses. The curve fit results indicate that the Pt–Pt first-shell coordination numbers and their interatomic distances are reasonable for the subnanometer-sized clusters. Pt_{17} and Pt_{19} showed almost similar coordination numbers relative to Pt_{13} (Figure 2d and Table S1), which corresponds to the low coordination number for the additional Pt atoms on the Pt_{13} core. A structural model for the Pt_{19} cluster with an icosahedral Pt_{13} core bearing three Pt dimers as edge sites was suggested from the optimized cluster structure using density functional theory (DFT) calculations. In addition, an aberration-corrected high magnification HAADF-STEM image of Pt_{19} supported the calculated structure (Figure 2b). Although a high flux of electron beam to the metastable clusters induced a continuous change of the atomic coordination image, some snapshots suggest a triangular cluster-shaped structure that is consistent with the calculated structure.

The electronic status of the as-synthesized clusters and that under in situ electrochemical conditions was determined. X-ray photoelectron spectroscopy (XPS) measurements (Pt $4f_{7/2}$) of the as-synthesized Pt_{13}, Pt_{17}, and Pt_{19} clusters supported the definite reduction of the platinum ions to zero-valency (Figure S4). In addition, the valence states during electrocatalysis are also available from analyses of the Pt L_3- and L_2-edge X-ray absorption near edge structure (XANES) spectra.[19] All XANES spectra were measured at a constant applied potential between 0.00 and 1.40 V versus Ag/AgCl in a 0.1 M aqueous perchloric acid using an in situ setup with the fluorescence mode. The total number of unoccupied d-states per platinum atom $(h_1)_{t,s}$ was calculated from each peak area of the white line (sharp peak near the absorption edge) in the XANES spectra.[20] At 0.00 V, when the platinum surface is generally reduced, all the subnanoparticle catalysts (Pt_{12}, Pt_{13}, Pt_{17}, and Pt_{19}) showed similar $(h_1)_{t,s}$ values to the larger platinum nanoparticle catalyst (commercial Pt/C catalyst for fuel cell applications), which is almost equivalent to that for bulk platinum metal (Table S2). In contrast, application of anodic potentials resulted in the removal of the d-electrons from the clusters, which could be observed as increases in the white line intensities. At a significantly high applied potential of 1.4 V, the XANES spectra were similar to those for platinum oxide (PtO_2). It should be noted that the original XANES spectra was again obtained when the applied potential was 0.0 V (Figure 2e), which suggests that the cluster structure is preserved, probably due to the structural elasticity. The behavior of the present clusters is equivalent to that reported for larger platinum nanoparticles.[21]

The accessibility of these subnanoparticle surfaces in **DPAG4-PyTPM** are sufficient for the catalytic reduction of oxygen.[6] Each of the as-synthesized subnanoparticles in the dendrimer reactor (**Pt_n@DPAG4-PyTPM**: $n = 12$–22) was modified on a glassy carbon electrode (GCE) to examine the dependence of the intrinsic catalytic activity on the atomicity. The catalytic activities for the electrochemical reduction of oxygen molecules were determined from rotating disk voltammetry (RDV) measurements in an oxygen-saturated aqueous solution of hydrogen perchlorate (0.1 mol L^{-1}) as the electrolyte using each modified GCE.[6] Linear sweep voltammograms to the negative potential exhibited a significant cathodic current characteristic of the electrochemical catalytic reduction of O_2. The currents were then converted to kinetic currents using the Koutecky–Levich equation to

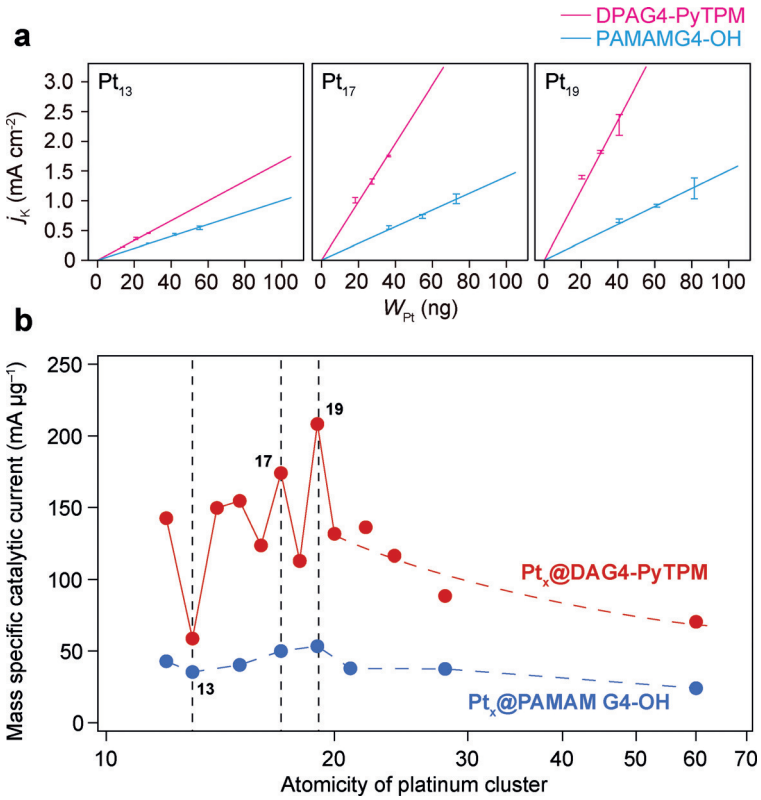

Figure 3. Catalytic activities for electrochemical oxygen reduction on platinum clusters with different atomicity. These clusters were synthesized using **PAMAM G4-OH** or **DPAG4-PyTPM** as templates. a) Observed catalytic current versus weight of the platinum modified on the electrode surface for Pt_{13}, Pt_{17}, and Pt_{19} clusters. b) Variations of the platinum-mass-specific catalytic activity versus the atomicity of the platinum clusters. Measurements were conducted under oxygen saturation in an acidic aqueous electrolyte (0.1 M $HClO_4$).

remove the diffusion-limiting current factor.[6] Measurement of the ORR for fuel cell applications is generally conducted using a Nafion membrane to facilitate the proton transfer process. However, the present measurements were conducted using the least amount of the platinum catalyst without the Nafion membrane to remove the effect of specific adsorption of the sulfonyl groups on the platinum surface and the rate-limiting step by oxygen migration through the thick Nafion and catalyst layers. By changing the weight of platinum from nanograms to micrograms, the mass-specific catalytic activity could be estimated from the slope of the Pt weight versus kinetic current plot (Figures 3a and S5).

The kinetic current was significantly dependent on the atomicity (Figure 3b). As previously reported, Pt_{13} has a much lower activity relative to Pt_{12}.[7] Other clusters also exhibited remarkable activities substantially higher than Pt_{13}. In particular, Pt_{19} had the highest activity among the available platinum clusters, of which the mass activity was 3.7 times higher than that of Pt_{13}. To confirm the origin of this catalytic activity, similar platinum clusters synthesized using **PAMAM G4-OH** were also studied using the same electrochemical procedure. Although the absolute catalytic activity was lower than that of the clusters synthesized with **DPAG4-PyTPM** as the template, probably due to the strict encapsulation,[22] the general trend showed an agreement with that of the clusters synthesized using **DPAG4-PyTPM**. In each case, the highest catalytic activity was also obtained with Pt_{19}, whereas the Pt_{13} cluster exhibited lower activities. The similar trend in the catalytic activity for the clusters synthesized using both dendrimers (**PAMAM G4-OH** and **DPAG4-PyTPM**) suggests that the unique activity of Pt_{19} and Pt_{13} is due to the intrinsic properties of the clusters, and not the dendrimer-specific interactions. However, the atomicity resolution obtained with **PAMAM G4-OH** seems to be lower relative to the clusters obtained with **DPAG4-PyTPM** because the dispersity in the number of precursor complexes in **PAMAM G4-OH** is ambiguous, whereas that in **DPAG4-PyTPM** involves a stepwise complexation process.

All the cluster structures from Pt_{13} to Pt_{19} are expected to have an icosahedral Pt_{13}-based kernel, as shown in the ESI-TOF-MS analyses. The reported $[Pt_{17}(CO)_{19}]^{-2}$ structure[23] based on an icosahedron core with two edges is in complete agreement with this assumption. On the other hand, the reported double icosahedral $[Pt_{19}(CO)_{17}]^{-8}$ structure[15] has a 232 CVE, which is slightly lower than the present value. This structure was not successfully converged in the structure optimization based on DFT calculations. Another possible structure expected from the high-magnification HAADF-STEM observation (Figure 2b) contains a single icosahedron appended with three edge sites,[24] which is reasonable for the observed 234 CVE and provided successful convergence in the structure optimization. Adatoms as dimers on a kernel is much more probable rather than distinct adatoms because the Pt_{15} having one dimer is more stable (32.9 kJ mol^{-1}) than the isomeric structure of Pt_{15} with two distinct platinum adatoms (trans-$Pt_{13}(Pt)_2$; Figure S6). Similar to the previous investigation,[7] the binding energy of an oxygen atom to each three-fold hollow site on the surface of the respective clusters, which is considered as an important factor for the ORR catalytic activity, was estimated by calculation.[25] All the cluster models having edges were suggested to have ideal oxygen binding energies near the edges, whereas the binding energies to the icosahedral kernels themselves were too strong. Figure 4 shows that the highly active sites are mainly located on the two sides of each sharp edge of the specific clusters (Pt_{15}, Pt_{17}, and Pt_{19}). In sharp contrast, the highly symmetric icosahedral Pt_{13} does not have any edge sites.

Based on these results, we can postulate that the stable Pt_{13} kernel (magic number cluster) does not have any significant activity, whereas adatoms on the stable kernel eventually exhibit high catalytic activity if they form edges. Castleman and colleagues suggested that the origin of the unique Al_{17}^- reactivity is mainly based on the geometric features rather than the electronic features. The geometric feature of Al_{17} with almost the same structure as the present

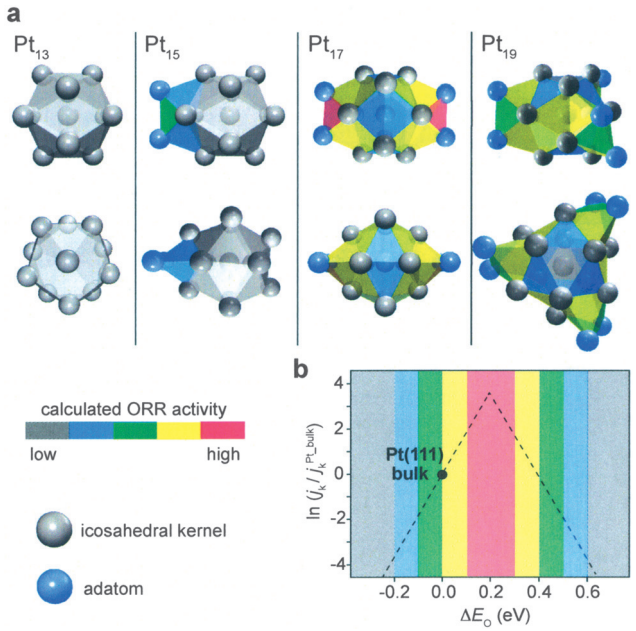

Figure 4. Possible atomicity-specific structures of platinum clusters that can reasonably explain the XAFS and catalytic activity results. a) Atomic coordination of platinum. b) Volcano diagram[25] for the oxygen binding energy to respective three-fold hollow sites. Platinum atoms as icosahedral kernels and adatoms are shown in different colors. The oxygen binding energies (ΔE_0) to each three-fold hollow site were determined from DFT calculations and converted to the ORR catalytic activities from the known volcano relationship. Ranges of the ORR activities are projected on the surfaces with the corresponding colors.

Pt_{17} arises from the contrastive role of each Al center on the edges and an icosahedral kernel that acts as an electron donor and acceptor, respectively.[3]

We can conclude that the dendrimer-based synthesis allows for the preparation of platinum clusters with various atomicities between 13 and 20 at very small dispersity ($\sigma < 2$). The catalytic activities for the ORR were significantly altered by the atomicity, despite this structural resemblance. In particular, Pt_{17} and Pt_{19} exhibited higher performance than the other series. DFT calculations and the experimental results suggest that such highly active clusters have edges as a common structural motif. The present findings have provided new insight into the subnanometer nonmagic number clusters, in that such superatomic molecules are potentially superior with respect to their unique heterogeneity. The catalyst ink of Pt_{60} on carbon (15 wt%) already shows better performance than the commercial Pt/C catalyst for ORR (Figure S8). The use of the present clusters as fuel cell catalysts is ongoing.

Keywords: catalysts · cluster compounds · dendrimers · oxygen reduction reaction · platinum

How to cite: *Angew. Chem. Int. Ed.* **2015**, *54*, 9810–9815
Angew. Chem. **2015**, *127*, 9948–9953

[1] a) S. Yamazoe, K. Koyasu, T. Tsukuda, *Acc. Chem. Res.* **2014**, *47*, 816; b) A. Taketoshi, M. Haruta, *Chem. Lett.* **2014**, *43*, 380.
[2] a) D. E. Bergeron, P. J. Roach, A. W. Castleman, N. O. Jones, S. N. Khanna, *Science* **2005**, *307*, 231; b) H. Häkkinen, *Chem. Soc. Rev.* **2008**, *37*, 1847; c) A. W. Castleman, Jr., S. N. Khanna, *J. Phys. Chem. C* **2009**, *113*, 2664.
[3] P. J. Roach, W. H. Woodward, A. W. Castleman, Jr., A. C. Reber, S. N. Khanna, *Science* **2009**, *323*, 492.
[4] a) Y. Negishi, T. Nakazaki, S. Malola, S. Takano, Y. Niihori, W. Kurashige, S. Yamazoe, T. Tsukuda, H. Häkkinen, *J. Am. Chem. Soc.* **2015**, *137*, 1206; b) Y. Shichibu, K. Suzuki, K. Konishi, *Nanoscale* **2012**, *4*, 4125.
[5] a) V. S. Myers, M. G. Weir, E. V. Carino, D. F. Yancey, S. Pande, R. M. Crooks, *Chem. Sci.* **2011**, *2*, 1632; b) L. M. Bronstein, Z. B. Shifrina, *Chem. Rev.* **2011**, *111*, 5301; c) R. M. Crooks, M. Zhao, L. Sun, V. Chechik, L. K. Yeung, *Acc. Chem. Res.* **2001**, *34*, 181.
[6] K. Yamamoto, T. Imaoka, W.-J. Chun, O. Enoki, H. Katoh, M. Takenaga, A. Sonoi, *Nat. Chem.* **2009**, *1*, 397.
[7] T. Imaoka, H. Kitazawa, W.-J. Chun, S. Omura, K. Albrecht, K. Yamamoto, *J. Am. Chem. Soc.* **2013**, *135*, 13089–13095.
[8] M. K. Debe, *Nature* **2012**, *486*, 43.
[9] Q. Cao, L. M. Dornan, L. Rogan, N. L. Hughes, M. J. Muldoon, *Chem. Commun.* **2014**, *50*, 4524.
[10] a) M. Shao, A. Peles, K. Shoemaker, *Nano Lett.* **2011**, *11*, 3714; b) E. Toyoda, R. Jinnouchi, T. Hatanaka, Y. Morimoto, K. Mitsuhara, A. Visikovskiy, Y. Kido, *J. Phys. Chem. C* **2011**, *115*, 21236.
[11] H. Kitazawa, K. Albrecht, K. Yamamoto, *Chem. Lett.* **2012**, *41*, 828.
[12] K. Yamamoto, T. Imaoka, *Bull. Chem. Soc. Jpn.* **2006**, *79*, 511.
[13] H. Ye, R. M. Crooks, *J. Am. Chem. Soc.* **2005**, *127*, 4930.
[14] M. P. Johansson, P. Pyykkö, *Chem. Commun.* **2010**, *46*, 3762.
[15] C. Femoni, M. C. Iapalucci, G. Longoni, S. Zacchini, S. Zarra, *J. Am. Chem. Soc.* **2011**, *133*, 2406.
[16] D. M. P. Mingos, *Acc. Chem. Res.* **1984**, *17*, 311.
[17] Y. Lei, H. Zhao, R. D. Rivas, S. Lee, B. Liu, J. Lu, E. Stach, R. E. Winans, K. W. Chapman, J. P. Greeley, J. T. Miller, P. J. Chupas, J. W. Elam, *J. Am. Chem. Soc.* **2014**, *136*, 9320.
[18] G. Longoni, P. Chini, *J. Am. Chem. Soc.* **1976**, *98*, 7225.
[19] M. Brown, R. Peierls, E. Stern, *Phys. Rev. B* **1977**, *15*, 738.
[20] A. N. Mansour, J. W. Cook, D. E. Sayers, *J. Phys. Chem.* **1984**, *88*, 2330.
[21] a) H. Yoshitake, O. Yamazaki, K. Ota, *J. Electrochem. Soc.* **1994**, *141*, 2516; b) M. Tada, S. Murata, T. Asakoka, K. Hiroshima, K. Okumura, H. Tanida, T. Uruga, H. Nakanishi, S. Matsumoto, Y. Inada, M. Nomura, Y. Iwasawa, *Angew. Chem. Int. Ed.* **2007**, *46*, 4310; *Angew. Chem.* **2007**, *119*, 4388.
[22] I. Nakamula, Y. Yamanoi, T. Yonezawa, T. Imaoka, K. Yamamoto, H. Nishihara, *Chem. Commun.* **2008**, 5716.
[23] S. S. Kurasov, N. K. Eremenko, Y. L. Slovokhotov, Y. T. Struchkov, *J. Organomet. Chem.* **1989**, *361*, 405.
[24] X.-K. Wan, Q. Tang, S.-F. Yuan, D.-e. Jiang, Q.-M. Wang, *J. Am. Chem. Soc.* **2015**, *137*, 652.
[25] a) J. Greeley, I. E. L. Stephens, A. S. Bondarenko, T. P. Johansson, H. A. Hansen, T. F. Jaramillo, J. Rossmeisl, I. Chorkendorff, J. K. Nørskov, *Nat. Chem.* **2009**, *1*, 552; b) D. Friebel, V. Viswanathan, D. J. Miller, T. Anniyev, H. Ogasawara, A. H. Larsen, C. P. O'rady, J. K. Nørskov, A. Nilsson, *J. Am. Chem. Soc.* **2012**, *134*, 9664.

Received: May 18, 2015
Published online: July 14, 2015